$k_t t_1 = 1.1$ yields a distribution nearly equal to the steady-state one for $\alpha = 0.85$, i.e. with $\mu^P(t_1) = 12.7$ and $\sigma^P(t_1) = 6.6$.

4. Conclusion

The main conclusions that can be drawn from the results obtained in this paper are as follows:

1. The transient distribution of products in Fischer–Tropsch synthesis and other catalytic polymerizations described by the rate equation 2.1 is very different from the steady-state distribution and may be readily accessible experimentally.

2. Under pulsed operating conditions it is therefore also possible to obtain product distributions that are very different from (i.e. much narrower than) those obtained under the usual steady-state operating conditions.

3. For Fischer–Tropsch synthesis, the differences are especially prominent and useful for catalysts with a growth rate parameter near unity (i.e. $\alpha \gtrsim 0.9$). For such catalysts it is possible to choose the pulse length so as to maximize the yield in the liquid-hydrocarbon range.

4. The results obtained under pulsed operating conditions can be used to determine the growth rate parameter α and the termination rate parameter k_t separately.

We end by noting that we have only considered pulsed operations in which all products are desorbed from the surface at the end of each full pulse. On can generalize the model to a situation in which a subsequent pulse begins before all adsorbed chains are desorbed. Such a model involves a greater number of operating parameters and will be considered elsewhere.[10]

Acknowledgment. We gratefully acknowledge very useful discussions with Dr. Olivia Rojas and Dr. V. Seshadri. This work was supported in part by a grant to K.L. from the Universitywide Energy Research Group of the University of California and by the National Science Foundation under Grant No. CHE-80-09816 (E.P.-L.).

Appendix

The standard deviation of $\sigma^P(t_1)$ for the pulsed experiment is given by

$$\frac{\sigma^P(t_1)}{\sigma^{ss}} = \frac{[N_1 + N_2 \exp(-k_t t_1) - N_3 \exp(-2k_t t_1)]^{1/2}}{N_4} \quad \text{(A1)}$$

where

$$N_1 \equiv k_t^2 t_1^2 - (5\alpha - 1)k_t t_1 + \alpha(6\alpha - 5) \quad \text{(A2)}$$

$$N_2 \equiv \tfrac{3}{2}\alpha^3 k_t^3 t_1^3 - \alpha^2(3\alpha^2 + \tfrac{7}{2}\alpha - 7)k_t^2 t_1^2 + \alpha(10\alpha^3 - 13\alpha^2 + 4\alpha + 5)k_t t_1 - \alpha(4\alpha^3 - 3\alpha^2 + 6\alpha - 5) \quad \text{(A3)}$$

$$N_3 \equiv \alpha^3[\tfrac{1}{2}\alpha^2 k_t^2 t_1^2 + (\alpha + 1)\alpha k_t t_1 - (4\alpha - 3)] \quad \text{(A4)}$$

and

$$N_4 \equiv k_t t_1 - (2\alpha - 1) + \alpha^2 \exp(-k_t t_1) \quad \text{(A5)}$$

Registry No. CO, 630-08-0.

EPR and ELDOR Studies on Spin Relaxation in Perdeuterated 2,2,6,6-Tetramethyl-4-piperidone-*N*-oxyl in Liquid Solutions. The Slowly Relaxing Local Structure Mechanism

E. van der Drift,* B. A. C. Rousseeuw, and J. Smidt

Delft University of Technology, Department of Applied Physics, 2600 GA Delft, The Netherlands
(Received: December 20, 1982; In Final Form: November 4, 1983)

The spin relaxation of perdeuterated 2,2,6,6-tetramethyl-4-piperidone-*N*-oxyl (PDT) in various solvents was studied via EPR line width and saturation and ELDOR. Saturation and ELDOR results are incompatible with the line-width results when the latter are analyzed in the standard manner: rotational diffusion (RD) with temperature invariance of the anisotropy factor N and of the non-Debye parameter ϵ in the nonsecular spectral densities $j(\omega_0)$. In a more general approach, first all relevant intramolecular relaxation terms are obtained independently from the combined T_2, T_1, and ELDOR data. Further analysis of these terms suggests that, in general, the rotational relaxation of PDT may arise from rotational diffusion (RD) and a slowly relaxing local structure mechanism (SRLS). Separation of RD and SRLS contributions seems possible via the electron spin relaxation rate, more particularly via the spin–rotational interaction part W_e^{SR}. This is most clearly shown by the results on PDT in methylcyclohexane (MCH) and in the isotropic phase of the liquid crystalline solvent 4′-*n*-octyl-4-cyanobiphenyl (8CB). Particularly, by virtue of the results on 8CB the combined T_2–T_1–ELDOR method seems promising in spin label/spin probe research on ordering media by its option to yield directly the ordering dynamics of the nearby environment.

Introduction

Careful relaxation studies on the nitroxide radicals peroxylaminedisulfonate (PADS)[1] and perdeuterated 2,2,6,6-tetramethylpiperidone-*N*-oxyl (PD-Tempone, PDT, see Figure 1)[2] in various media yielded detailed information about the molecular motion in terms of anisotropic reorientation and different rotational diffusion models. Particularly, deviations from the Brownian motion model were the main point of consideration. This is initiated by an anomalous frequency dependence of spectral densities and an unusual dynamical frequency shift in the motional narrowing region and by line-shape characteristics in the slow motional region. A unified explanation[3] of all these observations is obtained by considering the molecular reorientation as due to

(1) (a) S. A. Goldman, G. V. Bruno, and J. H. Freed, *J. Chem. Phys.*, **56**, 716 (1972); (b) *ibid.*, **59**, 3071 (1973).

(2) (a) J. S. Hwang, R. P. Mason, L. P. Hwang, and J. H. Freed, *J. Phys. Chem.*, **79**, 489 (1975); (b) C. F. Polnaszek and J. H. Freed, *ibid.*, **79**, 2283 (1975); (c) W. J. Lin and J. H. Freed, *ibid.*, **83**, 379 (1979); (d) S. A. Zager and J. H. Freed, *J. Chem. Phys.*, **77**, 3344 (1982); (e) S. A. Zager and J. H. Freed, *ibid.*, **77**, 3360 (1982); (f) L. L. Jones and R. N. Schwartz, *Mol. Phys.*, **43**, 527 (1981).

(3) (a) L. P. Hwang and J. H. Freed, *J. Chem. Phys.*, **63**, 118 (1975); (b) A. E. Stillman and J. H. Freed, *ibid.*, **72**, 550 (1980).

0022-3654/84/2088-2275$01.50/0

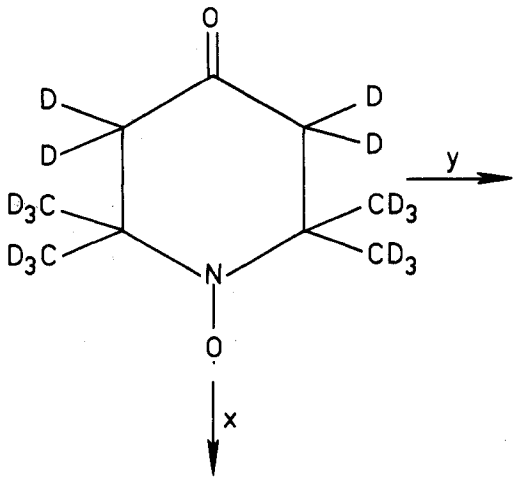

Figure 1. Molecular structure of PD-Tempone and the principal axis system for dipolar (D) and Zeeman (G) interactions.

a broad frequency spectrum of fluctuating torques with correlation time τ_M.

With the anisotropic reorientation of the spin probe described by several correlation times τ_i ($i = 0, \pm 2$)[1a] one distinguishes two parts in the torque spectrum: the fast components with $\tau_M \ll \tau_i$ which induce rotational diffusion (RD process) and more persistent components with $\tau_M \gg \tau_i$ which represent a slowly relaxing local structure (SRLS mechanism). Mostly, in the SRLS model the probe molecule is thought to experience a local ordering by the nearby environment which averages out in times $\tau_X \gg \tau_i$. In general, the reorientation of a spin probe will be the sum of RD and SRLS contributions and the spectral densities $j(\omega)$ can be written as[4]

$$j(\omega) = j_{RD}(\omega) + j_{SRLS}(\omega) \quad (1)$$

The relative importance of both parts depends on the relative size of the probe and solvent molecules as well as the structure of the solvent itself. The intermediate region of fluctuating torques ($\tau_M \approx \tau_I$) can be taken into account via an anomalous formulation of the spectral density $j_{RD}(\omega)$. According to Hwang[2a] one has

$$j_{RD_i}(\omega) = j_{RD_i}(0)/(1 + \epsilon\omega^2\tau_i^2) \quad (2)$$

with $\epsilon > 1$ due to components with $\tau_M \approx \tau_i$; $j_{RD_i}(0)$ is the ith term within $j_{RD}(0)$ corresponding to τ_i. In nitroxide radicals we have spectral densities $j(\omega)$ at zero frequency, $\omega_n = 1.3 \times 10^8$ s^{-1}, and X-band EPR frequency, $\omega_0 = 5.6 \times 10^{10}$ s^{-1}, hereafter to be indicated by secular (S), pseudosecular (PS), and nonsecular (NS) terms, respectively.

Although the torque model is a valuable refinement of the existing relaxation theory and accounts for the noted anomalies, it leads also to more ambiguity in practical line-width studies. In fitting experimental results to

$$T_2^{-1} = A + Bm + Cm^2 \quad (3)$$

only the coefficients B and C can be accurately interpreted by spectral terms $j(\omega)$, whereas the full torque model requires an excess of parameters: the principal components of the rotational diffusion tensor **R**, which underlie the various τ_i, including their positioning in the molecular frame; the local ordering parameter and its correlation time τ_X; the parameters ϵ and ϵ' for the nonsecular and pseudosecular terms $j(\omega)$, respectively. In this context it was pointed out by Hwang et al.[5] that, in general, one needs a total reanalysis of spin relaxation data as a result of modified τ_i values due to SRLS contributions. Only rough estimates of the SRLS parameters were obtained there because of the limited data. Earlier attempts[1b,2a,6] to obtain complementary information from saturation studies were somewhat unsuccessful in the sense that they rather led to more complications: the magnitude of the electron spin relaxation rate W_e was found to be anomalously large on the basis of the existing relaxation theory. More recent theoretical formulations of W_e leave this essentially unchanged.[2a,3b]

The essential point of the present work is that with line width, saturation, and ELDOR measurements together, sufficient data can be obtained to justify such a complete reanalysis. Hwang et al.[2a] first pointed out the important role which ELDOR could play in providing additional information to correctly analyze the spin relaxation data. In this work we utilize the fact that the ELDOR response is an additional and independent probe for the pseudosecular and nonsecular contributions to the relaxation pattern.

The present study deals with line width, T_1, and ELDOR measurements on PDT in several ordinary solvents and is then closely related to the fast motional part of experimental studies on PDT cited above. Very recently, Popp and Hyde[7] reported such a combined study via line-width, saturation recovery, and ELDOR measurements on a nitroxide radical in a model membrane. In their analysis based exclusively upon RD contributions, they report also the unusually large W_e as well as an inconsistency between EPR line-width and the combined ELDOR–saturation recovery results. In our study on PDT we find similar discrepancies. It leads us to follow a more general approach where as a first step all spectral densities $j(\omega)$ and the rate W_e are determined independently from the combined results. As most striking feature we find in some solvents the inequality $j(0) > j(\omega_n)$ although certainly the motional narrowing condition applies, i.e., $j_{RD}(\omega_n) = j_{RD}(0)$ in a very good approximation. To explain this we have considered the full torque model since in the motional narrowing region one might still have $j_{SRLS}(0) > j_{SRLS}(\omega_n)$ due to $\tau_X \approx \omega_n^{-1}$. Beside this we suggest how such an analysis could give a new meaning to the generally observed discrepancy between experimental and calculated W_e rates.

Experimental Section

Sample Preparation. PDT was prepared by a method differing somewhat from the procedure of Rozantsev.[8] In order to avoid handling with liquid ammonia (ND_3) in an autoclave, the synthesis was performed with a concentrated (20%) ammonia (ND_3) solution in D_2O under addition of a large amount of anhydrous $CaCl_2$. More specifically, we start with a mixture of 30 mL of acetone-d_6 (Merck) and 35 g of anhydrous $CaCl_2$. After the solution was cooled to 238 K, 27.5 mL of the ammonia solution (Fluka, Baker) and 25 g of $CaCl_2$ were added. After the mixture was further cooled to 203 K and subsequently warmed (slowly, 36 h) to room temperature under well-isolated conditions the reaction was left to proceed for about 1 week. Other reaction steps and final isolation of PDT as described by Rozantsev[8] were used. The yield was 13%. Samples of PDT in toluene (TO), *sec*-butylbenzene (SBB), methylcyclohexane (MCH), and the liquid crystal 4′-*n*-octyl-4-cyanobiphenyl (8CB) (BDH Chemicals Ltd.) were prepared in vacuo with carefully dried and deoxygenated solvents. The 8CB sample was degassed while in the isotropic phase ($T > 314$ K). For measuring the intramolecular relaxation special care was taken to optimize the radical concentration in order to find the best compromise between a maximum S/N ratio and a minimum intermolecular relaxation. All results in this work are from radical concentrations of about 7×10^{-5} mol/L. Then, electron spin exchange is small whereas intermolecular electron dipolar terms are found to be negligible. We used 5-mm o.d. NMR sample tubes and a solvent column length of about 16 mm.

EPR/ELDOR Spectrometer. EPR/ELDOR measurements were performed on a homebuilt spectrometer[9] operating in the

(4) J. H. Freed, *J. Chem. Phys.*, **66**, 4183 (1977).
(5) J. S. Hwang, K. V. S. Rao, and J. H. Freed, *J. Phys. Chem.*, **80**, 1490 (1976).
(6) P. W. Percival and J. S. Hyde, *J. Magn. Reson.*, **23**, 249 (1976).
(7) C. A. Popp and J. S. Hyde, *Proc. Natl. Acad. Sci. U.S.A.*, **79**, 2559 (1982).
(8) E. G. Rozantsev, "Free Nitroxyl Radicals", Plenum Press, New York, 1970.
(9) A. F. Mehlkopf, F. G. Kuiper, J. Smidt, and T. A. Tiggelman, *Rev. Sci. Instrum.*, **54**, 695 (1983).

TABLE I: Magnetic Interactions in PDT

interaction (nucleus)		SBB I[a]	SBB II[b]	MCH I[a]	MCH II[b]
dipolar (N)	A_{xx}, mT	0.47 ± 0.05	0.70 ± 0.05	0.46 ± 0.05	0.80 ± 0.05
	A_{yy}, mT	0.57 ± 0.05	0.32 ± 0.05	0.56 ± 0.05	0.20 ± 0.05
	A_{xx}, mT	3.35 ± 0.02	3.35 ± 0.02	3.31 ± 0.02	3.65 ± 0.03
Zeeman	g_{xx}	2.0095 ± 0.0002	2.0102 ± 0.0003	2.0096 ± 0.0002	2.0096 ± 0.0002
	g_{yy}	2.0062 ± 0.0002	2.0055 ± 0.0003	2.0062 ± 0.0002	2.0062 ± 0.0002
	g_{zz}	2.0022 ± 0.0001	2.0022 ± 0.0001	2.0022 ± 0.0001	2.0022 ± 0.0001
isotropic coupling (D)	a_D, μT	2.47 ± 0.05		3.0 ± 0.1	

[a] These species are used in further analysis of the relaxation data. [b] These species appear in rigid limit analysis but are not used in further analysis.

absorption mode with 10-kHz field modulation. In this study we used the B_0–ν_p–ELDOR sweep mode, i.e., with the pumping frequency ν_p in resonance during the magnetic field sweep. The temperature in the cavity was controlled by standard variable-temperature accessories, giving a long-term stability of about 0.5 °C. In absolute value the accuracy of the temperature is about 1 °C.

Line-Width Measurements. The three EPR lines in the spectrum of PDT are inhomogeneously broadened by the hyperfine coupling a_D with the 12 equivalent deuterons of the four CD_3 groups. The hyperfine splitting of the four ring deuterons is much smaller and can be ignored. The intrinsic width of the three inhomogeneously broadened lines is deduced from the overall width of the central line ($m = 0$) and the three peak-to-peak heights by using the method of Hwang et al.[2a] To that purpose one should know a_D which is found from a line-shape analysis. Results for a_D in MCH and SBB are mentioned in Table I. Values in TO and 8CB are given elsewhere.[2a,2c] Throughout the experiments the microwave field was kept low in order to avoid saturation. Similarly the modulation of the magnetic field was below the level of distorting the line shape. The three intrinsic width were fitted to eq 3 yielding A, B, and C.

T_1 Measurements. T_1 data were obtained from CW saturation experiments by using the method of Hwang et al.[2a] The inhomogeneity of the microwave field H_1 and the modulation field H_m was taken into account by using the T_1 result of Hwang et al. on PDT in perdeuterated toluene[2a] at 211.7 K as an absolute standard. The well-defined standard of PADS in aqueous solution at 20 °C could not be used on account of the sample diameter of 5 mm.

ELDOR Measurements. The ELDOR response is described in terms of a reduction factor $R_{i,j}$, defined as the fractional change in the intensity of line i due to pumping (P) another line j.[10] In formula

$$R = \frac{\mathrm{EPR}(P=0) - \mathrm{EPR}(P\neq 0)}{\mathrm{EPR}(P=0)} \qquad (4)$$

The reduction factor $R_{i,j}^{\infty}$ at infinite pumping power (P), which can be found by extrapolation in plots of $R_{i,j}$ vs. P^{-1} is of particular interest because it depends merely on the relaxation.[10] Experimental methods, including a description of the equipment and a correction procedure for inhomogeneous broadening and instrumental effects in these plots, but adjusted to the field-pumping frequency ($B_0 - \nu_p$) sweep ELDOR mode, are given elsewhere.[11]

Results

Rigid Limit Spectra and Magnetic Parameters. The results for the dipolar tensor **A** and the Zeeman tensor **g** for PDT in MCH and SBB are given in Table I. The data are from our own measurements and a standard analysis[12] by computer simulation. Results for TO and 8CB are given by Hwang[2a] and Lin.[2c]

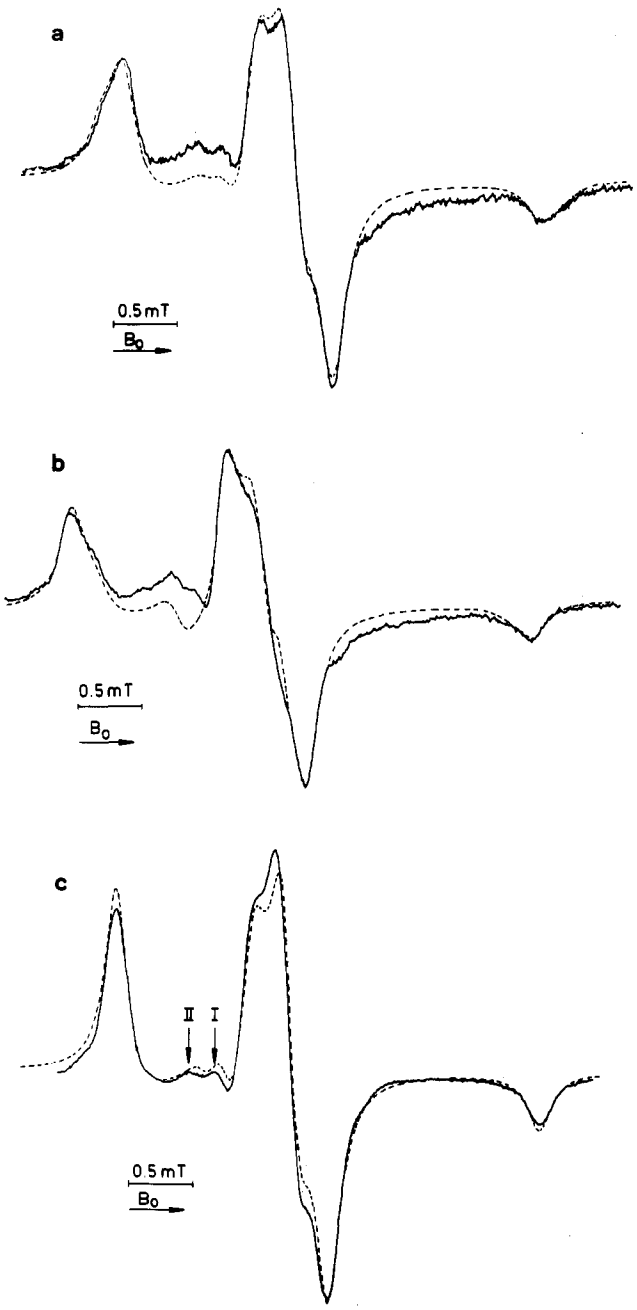

Figure 2. Experimental (—) and computer-simulated (– – –) rigid limit spectra of PDT in perdeuterated MCH (a,b) at 100 K and in SBB (c) at 120 K. Simulations involve a mixture of two species (I and II, see arrows in c). See text.

Within the frame of this work we make a few comments on the role of the surrounding solvent structure. This is most clearly justified for MCH (perdeuterated for reasons of spectrum reso-

(10) M. P. Eastman, G. V. Bruno, and J. H. Freed, *J. Chem. Phys.*, **52**, 321 (1970).
(11) E. van der Drift, A. J. Dammers, and J. Smidt, *J. Magn. Reson.*, **40**, 551 (1980).
(12) C. F. Polnaszek, Ph.D. Thesis, Cornell University, 1976.

lution) where two different species are always found, hereafter indicated by I and II. Their relative importance in a particular rigid limit spectrum depends on the method of cooling. The spectrum shown in Figure 2a is obtained by rapid cooling to 100 K, then warming to ca. 130 K until the glassy state was replaced by the polycrystalline phase and finally cooled again to 100 K. The spectrum shown in Figure 2b is obtained by cooling directly to 100 K. Detailed simulation shows that the spectra consist of 70% species I and 30% species II (Figure 2a) or vice versa (Figure 2b). The A components of species I correspond to the isotropic hyperfine splitting a_N observed in ELDOR at much higher temperatures and throughout this work species I will be used in further analysis. Possibly species II represents PDT molecules which are forced into a particular conformation due to close packing of solvent molecules. Additional support to this idea is given elsewhere[13] by rigid limit spectra of a perdeuterated spin probe in different liquid-crystalline solvents. The broad background around the center in Figure 2, a and b, may be associated with clustering of radicals.[1a,14]

The summation of spectra originating from different species of PDT in MCH leads to a calculated absorption line shape which in the field range between the low-field peak and the central line is very similar to the experimental line shape observed in that field range for PDT in SBB (Figure 2c). Simulations on the basis of one species show invariably the discrepancy which is observed and commented on elsewhere in other solvents.[2] Simulations on the basis of two components (Figure 2c; 70% I and 30% II) yield a much better agreement. Obviously, PDT exists in at least two conformations when frozen out in the rigid limit. Following the outline given elsewhere[2a] the consequences of a summation of different species for the interpretation of relaxation data can be neglected and throughout this work species I is used in further analysis.

Line Width. EPR line-width results for PDT at different temperatures in the four solvents were fitted to eq 3 yielding A, B, and C. Most information is obtained from coefficients B and C. Results for B and C in SBB, MCH, and 8CB are plotted in Figure 3 a–c, respectively, together with the calculated results to be explained below. Results on PDT in TO are very similar to those reported by Hwang[2a] and will not be mentioned.

Saturation and ELDOR. T_1 results from saturation measurements on PDT in the four solvents are collected in Table II together with the calculated results to be discussed below. Similarly in Tables III–IV we show experimental ELDOR reduction factors of PDT in TO, SBB, MCH, and 8CB, respectively, together with calculated results to be explained later on.

Analysis

Preliminary Considerations. Firstly the line-width, T_1, and ELDOR results are analyzed in a standard manner.[1,15] One starts with the classical description[1] of the line-width coefficients B and C under axially symmetric rotational diffusion yielding the mean correlation time $\bar{\tau} = 1/(R_\parallel R_\perp)^{1/2}$ with a constant value of $N_\alpha = N_\parallel/N_\perp$, ϵ, and ϵ' in the given temperature range. $R_\parallel$ and $R_\perp$ are the components of **R** parallel and perpendicular to the symmetry axis of reorientation (α) which for PDT can be assumed to coincide with one of the principal axes x, y, or z of the molecular frame shown in Figure 1. Next, the T_1 and ELDOR results are described[15] via the longitudinal relaxation pattern shown in Figure 4. Beside relaxation terms from dipolar (D) and mixed dipolar–Zeeman (DG) origin, it includes intermolecular relaxation by electron spin exchange (W_{ex}) and electron spin relaxation ($W_e^{(0)}$). Quadrupolar relaxation is neglected because ENDOR results[16] point to a quadrupole coupling of about −2.5 MHz which is small compared with the dipolar anisotropy. When the outcome

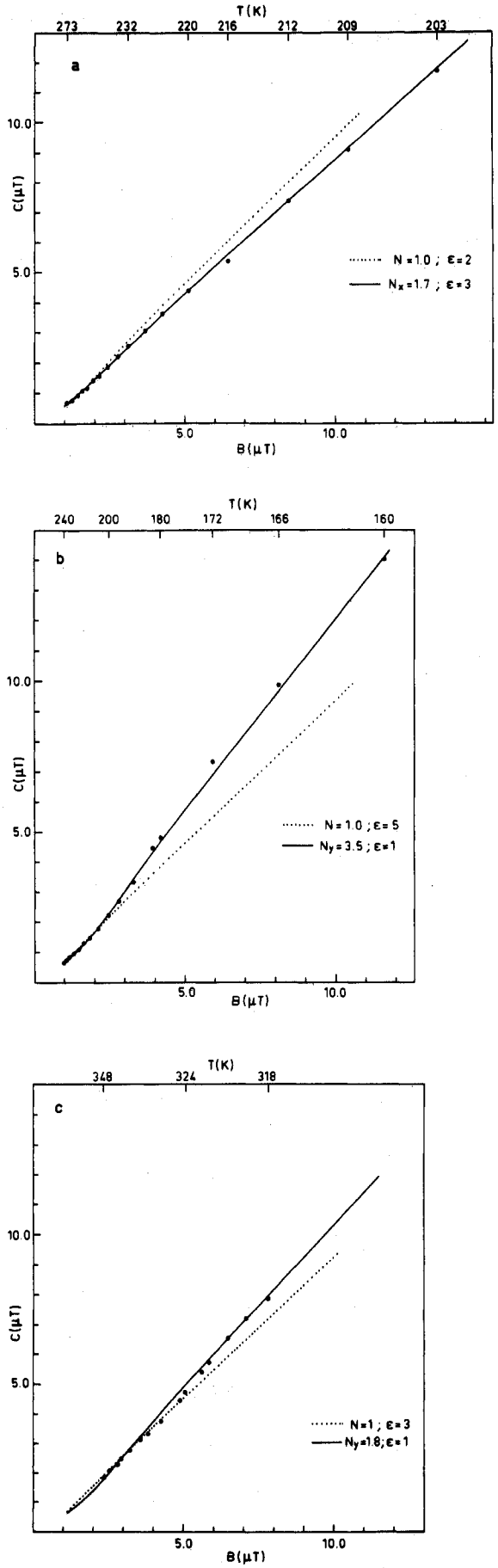

Figure 3. A comparison of experimental (●) and calculated line-width parameters B vs. C for PDT in SBB (a), MCH (b), and 8CB (c) at X-band frequency.

(13) E. Meirovitch, D. Igner, E. Igner, G. Moro, and J. H. Freed, *J. Chem. Phys.*, **77**, 3915 (1982).
(14) R. Pathasarathy, K. J. Rao, and C. N. R. Rao, *J. Phys. Chem.*, **85**, 3085 (1981).
(15) J. H. Freed, "Multiple Electron Resonance Spectroscopy", M. M. Dorio and J. H. Freed, Eds., Plenum Press, New York, 1979, Chapter III.
(16) K. P. Dinse, K. Möbius, M. Plato, R. Biehl, and H. Haustein, *Chem. Phys. Lett.*, **14**, 196 (1972).

TABLE II: Experimental and Calculated T_1 (s) for PDT in TO, SBB, MCH, and 8CB

		$T_1(m=1)$		$T_1(m=0)$			$T_1(m=-1)$	
			calcd[b]		calcd[b]			calcd[b]
solvent	T, K	expt[a]	(G)	expt[a]	$N-\epsilon$	G	expt[a]	(G)
TO	233	10.5	10.8	9.4	3.0	9.4	8.6	8.4
	223	9.8	10.5	9.1	6.4	8.6	8.4	8.2
	216	11.3	11.7	9.5	6.9	9.2	9.3	9.2
	211	11.9	12.4	9.6	7.4	9.5	10.2	9.8
	204	13.1	13.2	9.5	7.9	9.6	10.8	10.6
	198	13.1	13.7	10.0	8.6	10.0	12.0	11.4
	193	13.4	13.8	10.6	8.9	10.3	11.8	11.8
	188	13.4	14.0	10.9	9.4	10.9	12.9	12.4
SBB	238	9.1	9.6	8.5	6.4	8.0	8.1	8.1
	235	9.5	10.0	8.5	6.8	8.1	8.3	8.3
	230	9.4	10.0	8.2	7.4	7.8	8.3	8.2
	225	11.4	12.2	9.4	7.6	9.2	10.6	10.2
	223	10.7	11.1	8.5	7.6	8.3	9.4	9.3
	220	11.9	12.3	9.3	7.9	9.1	10.4	10.3
	215	12.2	12.7	9.4	9.0	9.4	11.2	10.9
	210	12.2	12.0	9.5	9.9	9.3	10.6	10.7
MCH	206	10.2	10.4	9.0	7.3	8.7	8.3	8.4
	199	11.0	11.3	9.3	8.1	9.0	8.9	8.9
	193	12.2	12.1	9.6	7.3	9.4	9.7	9.8
	186.5	12.7	12.6	9.8	8.0	9.5	10.3	10.4
	179.5	14.6	14.4	11.3	7.9	10.7	11.4	11.8
	173	13.1	13.0	10.2	8.5	9.8	10.8	10.8
8CB	324	6.3	6.5	5.2	3.5	5.1	5.6	5.5
	320	6.9	7.0	5.6	3.3	5.4	6.1	6.1
	317	6.8	7.1	5.6	2.5	5.4	5.8	6.1

[a] Experimental accuracy ±7%. [b] $N-\epsilon$ refers to calculated values based upon the classical analysis of the line width. See text. G refers to calculated values based upon the general approach. See text.

of the line-width analysis only is used, $W_e^{(0)}$ and W_{ex} are unknown. $W_e^{(0)}$ is most accurately found by optimizing the reconstruction of ELDOR reduction factors, while W_{ex} is obtained by refining this ELDOR fit for $R_{1,-1}$ and $R_{-1,1}$ which in the absence of W_{ex} obey the relation

$$R_{m,0}R_{0,m'} = R_{m,m'} \quad (m = -m' = \pm 1) \tag{5}$$

Finally, with all relaxation rates known from T_2 and ELDOR, the experimental T_1 can be compared with calculated T_1 in order to check the internal consistency. The outcome of this procedure

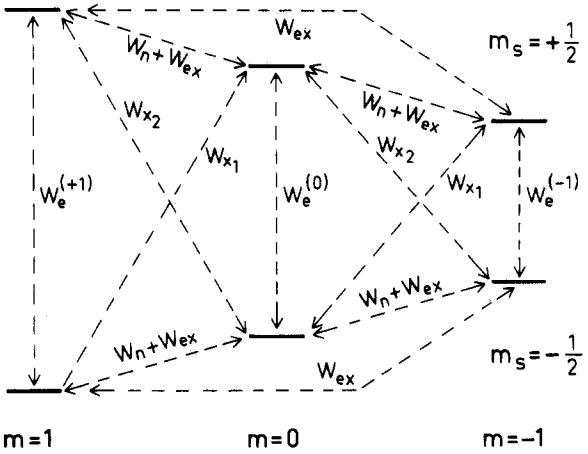

Figure 4. Energy level diagram of the electron–^{14}N ($I = 1$) system showing the possible relaxation paths: $W_n = j^{DD}(\omega_n)$; $W_{x_2} = 6W_{x_1} = 4j^{DD}(\omega_0)$; $W_e^{(m)} = W_e^{(0)} + 4j^{DG}(\omega_0)B_0m + 2j^{DD}(\omega_0)m^2$; W_{ex} represents the nuclear relaxation due to electron spin exchange.

may be summarized as follows:

1. The standard line-width analysis for PDT in SBB, MCH, and 8CB is shown in Figure 3. The fully drawn curves of calculated B vs. C show the best agreement with the experimental points. The dotted curves, however, illustrate the ambiguous character of line-width interpretations when N and ϵ are taken to be temperature dependent. The parameter ϵ' is insignificant because throughout this work $\bar{\tau} < 2 \times 10^{-10}$ s and then, very accurately, $j_{RD}{}^{DD}(0) = j_{RD}{}^{DD}(\omega_n)$. Our results for PDT in TO are similar to those reported by Hwang,[2a] i.e., $N \approx 1$ and $\epsilon \approx 5$.

2. In general, the experimental T_1 values are larger than the calculated $(N-\epsilon)$ ones. This is shown in Table II for the T_1 of the central line. Particularly in 8CB the discrepancy is substantial, but it also occurs in TO and SBB when nonsecular terms are important.

3. Certain asymmetry features in the T_1 and ELDOR pattern, e.g., $R_{1,0}$ vs. $R_{-1,0}$ or $T_1^{(+1)}$ vs. $T_1^{(-1)}$, are insufficiently accounted for. See Figure 5 where for TO calculated ratios $R_{1,0}/R_{-1,0}$ and $R_{1,-1}/R_{1,1} = (T_1^{(+1)}/T_1^{(-1)})^{15}$ are compared with the experimental results. According to the relaxation pattern in Figure 4 it points to an underestimated of the value for $j^{DG}(\omega_0)B_0$ in

$$W_e^{(m)} = W_e^{(0)} + 2j^{DD}(\omega_0)m^2 + 4j^{DG}(\omega_0)B_0m \tag{6}$$

In SBB and 8CB similar tendencies have been noticed. Summarizing, we are lead to suggest a more general approach where

TABLE III: Experimental and Calculated ELDOR Reduction Factors of PDT in TO

		reduction factors R_{ij}^{∞},[a] %					
T, K		$R_{1,0}$	$R_{-1,0}$	$R_{0,1}$	$R_{0,-1}$	$R_{1,-1}$	$R_{-1,1}$
233	expt	5.6 ± 0.2	4.6 ± 0.2	4.9 ± 0.2	5.2 ± 0.3	3.8 ± 0.2	3.1 ± 0.2
	G	5.8	4.5	5.0	5.0	3.6	2.8
223	expt	12.4 ± 0.4	9.5 ± 0.3	10.1 ± 0.1	10.6 ± 0.2	4.2 ± 0.2	3.2 ± 0.1
	G	12.3	9.7	10.1	10.2	4.4	3.4
216	expt	19.0 ± 0.6	15.2 ± 0.4	16.0 ± 0.4	15.5 ± 0.5	5.8 ± 0.2	4.5 ± 0.3
	G	19.4	15.5	15.4	15.5	6.1	4.8
211	expt	24.3 ± 0.5	20.4 ± 0.4	19.9 ± 0.4	19.9 ± 0.3	7.5 ± 0.3	6.1 ± 0.2
	G	25.0	20.1	19.2	19.5	7.7	6.1
204	expt	36.8 ± 0.5	31.6 ± 0.7	29.0 ± 0.3	30.4 ± 0.8	13.5 ± 0.4	10.8 ± 0.4
	G	38.3	31.5	28.2	28.9	13.5	10.9
198	expt	49.7 ● 0.6	43.9 ± 0.8	39.0 ± 0.7	40.7 ± 0.6	20.6 ± 0.7	17.8 ± 0.5
	G	51.3	43.8	37.5	38.7	21.7	17.9
193	expt	60 ± 2	54.9 ± 0.9	45.5 ± 0.3	48 ± 2	32 ± 2	25.8 ± 0.5
	G	61.9	54.6	46.0	47.7	30.8	26.2
188	expt	73 ± 2	67 ± 2	58 ± 2	63 ± 3	47 ± 2	40 ± 2
	G	74.9	68.7	58.5	60.7	46.1	40.8

[a] The indices i and j refer to observed and pumped line, respectively. G refers to calculated values based upon the general approach. See text. The experimental accuracies are based upon a least-squares analysis in plots of R^{-1} vs. P^{-1}.

TABLE IV: Experimental and Calculated ELDOR Reduction Factors of PDT in SBB

		reduction factors $R_{i,j}^{\infty}$,[a] %					
T, K		$R_{1,0}$	$R_{1,0}$	$R_{0,1}$	$R_{0,-1}$	$R_{1,-1}$	$R_{-1,1}$
238	expt	14.4 ± 0.3	12.9 ± 0.4	12.6 ± 0.2	12.2 ± 0.3	3.4 ± 0.1	2.9 ± 0.1
	G	14.8	12.5	12.3	12.3	3.4	2.9
235	expt	17.2 ± 0.2	14.8 ± 0.4	15.4 ± 0.3	14.2 ± 0.2	4.0 ± 0.1	3.4 ± 0.1
	G	17.9	15.0	14.4	14.5	4.0	3.4
230	expt	24.3 ± 0.3	20.5 ± 0.2	19.9 ± 0.4	19.2 ± 0.4	6.4 ± 0.1	5.1 ± 0.1
	G	24.5	20.3	19.0	19.2	6.2	5.1
225	expt	33.8 ± 0.3	28.9 ± 0.5	26.7 ± 0.4	27.2 ± 0.5	10.4 ± 0.3	8.3 ± 0.3
	G	34.6	29.4	26.0	26.4	10.4	8.7
223	expt	36.4 ± 0.4	32.3 ± 0.9	29.5 ± 0.8	28.0 ± 0.6	11.7 ± 0.7	10.3 ± 0.2
	G	37.2	31.0	27.8	28.3	11.7	9.8
220	expt	44.0 ± 0.7	38.8 ± 0.8	34.5 ± 0.4	34.6 ± 1.0	16.2 ± 0.4	13.9 ± 0.5
	G	45.5	39.9	33.5	34.3	16.8	14.1
215	expt	59 ± 2	54 ± 2	44.7 ± 0.9	45.0 ± 0.9	26.3 ± 0.9	22.0 ± 0.4
	G	58.9	52.3	43.7	45.1	27.4	23.6
210	expt	68 ± 2	69 ± 2	57 ± 2	58 ± 2	41 ± 3	36.8 ± 0.4
	G	71.9	66.1	55.7	57.5	41.8	37.2

[a] The calculated values refer to the general approach. [b] Experimental accuracies are based upon a least-squares analysis in plots of R^{-1} vs. P^{-1}.

TABLE V: Experimental and Calculated ELDOR Reduction Factors of PDT in MCH

		reduction factors $R_{i,j}^{\infty}$,[a] %					
T, K		$R_{1,0}$	$R_{-1,0}$	$R_{0,1}$	$R_{0,-1}$	$R_{1,-1}$	$R_{-1,1}$
206	expt	9.9 ● 0.3	7.9 ± 0.2	9.2 ± 0.2	8.9 ± 0.5	2.3 ± 0.5	2.0 ± 0.1
	G	10.2	8.3	8.6	8.6	2.4	2.0
199	expt	17.0 ± 0.3	12.1 ± 0.4	13.2 ± 0.4	13.3 ± 0.6	3.9 ± 0.2	3.3 ± 0.2
	G	16.5	13.2	13.2	13.3	4.1	3.2
193	expt	22.9 ± 0.4	19.4 ± 0.8	20.3 ± 0.3	19.1 ± 0.4	6.9 ± 0.5	5.6 ± 0.1
	G	23.9	19.5	18.6	18.8	7.2	5.8
186.5	expt	38.5 ± 1.0	31.8 ± 0.7	29 ± 2	28.7 ± 0.5	14.0 ± 0.3	12.2 ± 0.2
	G	38.4	32.2	28.8	29.5	14.5	11.9
179.5	expt	47 ± 2	39 ± 2	37.9 ± 0.6	37.5 ± 1.0	23.5 ± 0.8	17.3 ± 0.4
	G	48.2	40.9	36.0	37.2	22.4	18.4
173	expt	61.4 ± 0.6	52 ± 2	49 ± 3	48.2 ± 0.9	34 ± 2	29.4 ± 0.7
	G	61.8	53.8	46.7	48.8	34.9	29.1

[a] The calculated values refer to the general approach. [b] Experimental accuracies are based upon a least-squares analysis in plots of R^{-1} vs. P^{-1}.

TABLE VI: Experimental and Calculated ELDOR Reduction Factors in 8CB (I Phase)

		reduction factors $R_{i,j}^{\infty}$,[a] %					
T, K		$R_{1,0}$	$R_{-1,0}$	$R_{0,1}$	$R_{0,-1}$	$R_{1,-1}$	$R_{-1,1}$
324	expt	20.6 ± 0.6	18 ± 1	16.7 ± 0.2	17.1 ± 0.7	4 ± 1	5 ± 1
	G	21.2	18.3	16.9	16.9	3.6	3.1
320	expt	28 ± 1	23.9 ± 0.6	22.5 ± 0.2	23 ± 1	6.1 ± 0.5	5.5 ± 0.6
	G	28.3	24.6	21.8	22.0	6.2	5.4
317	expt	29 ± 1	24 ± 1	23.3 ● 0.8	25 ± 2	7.2 ± 0.4	6.7 ± 0.6
	G	29.2	25.5	22.5	22.7	6.6	5.7

[a] The calculated values refer to the general approach. [b] Experimental accuracies are based upon a least-squares analysis in plots of R^{-1} vs. P^{-1}.

first the various $j(\omega)$ and $W_e^{(0)}$ are evaluated independently and next the motional model is developed from these relaxation terms.

Evaluation of Relaxation Terms. The procedure involves three steps:

1. The dimensionless ELDOR reduction factors are analyzed. On the basis of the relaxation scheme in Figure 4 these factors are most conveniently described by the parameters

$$\overline{j^{DD}(\omega_n)}, \quad \overline{j^{DD}(\omega_0)}, \quad \overline{j^{DG}(\omega_0)B_0} \quad \overline{W_{ex}} \qquad (7)$$

where the bar denotes a normalization to $W_e^{(0)}$. It is a numerical problem which is further explained in the Appendix.

2. $T_1^{(m)}$ is reconstructed by using the solution of set (7). It yields $W_e^{(0)}$ and so all other $j(\omega)$ in the relaxation scheme of Figure 4.

3. The line-width coefficients B and C are analyzed via[1,2]

$$B = (16/3)j^{DG}(0)B_0 + 4j^{DG}(\omega_0)B_0 \qquad (8)$$

$$C = (8/3)j^{DD}(0) - j^{DD}(\omega_n) - (1/3)j^{DD}(\omega_0) \qquad (9)$$

which yields the secular terms $j^{DD}(0)$ and $j^{DG}(0)B_0$ after substitution of known $j(\omega)$ from previous steps. Calculated $T_1^{(m)}$ and

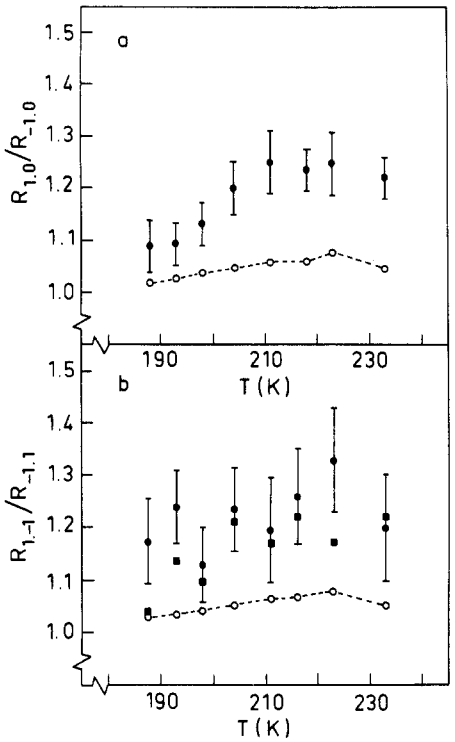

Figure 5. Experimental (●) and calculated (○) ratios of ELDOR reduction factors of PDT in TO. See text: (a) $R_{1,0}/R_{-1,0}$; (b) $R_{1,-1}/R_{-1,1}$; on account of the theoretical equality $R_{1,-1}/R_{-1,1} = T_1^{(+1)}/T_1^{(-1)}$ experimental ratios $T_1^{(+1)}/T_1^{(-1)}$ (■) are included. Experimental accuracies in the T_1 ratio and $R_{1,-1}/R_{-1,1}$ are about equal.

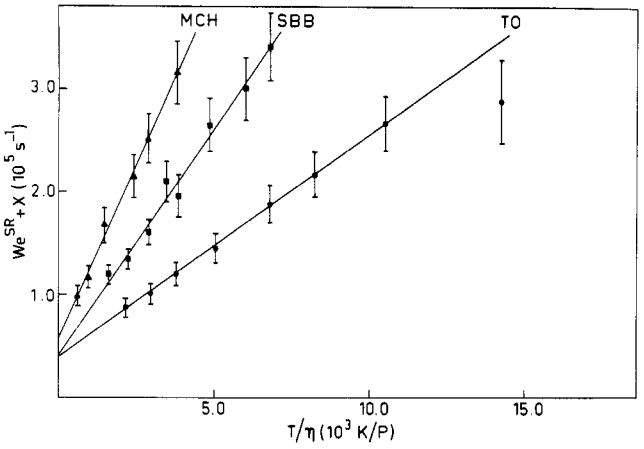

Figure 6. Least-squares plot of experimental ($W_e^{SR} + X$) vs. T/η for PDT in TO, SBB, and MCH. X values obtained are $(4.0 \pm 0.3) \times 10^4$ s^{-1} (TO), $(4.2 \pm 1.0) \times 10^4$ s^{-1} (SBB), and $(5.7 \pm 0.6) \times 10^4$ s^{-1} (MCH).

$R_{m,m'}$ are shown in Tables II–VI while the relaxation terms, which are most relevant for further analysis, are collected in Table VII.

A very useful quantity is the spin–rotational interaction term W_e^{SR} which is obtained by further analysis of the relaxation rate $W_e^{(0)}$ according to[15]

$$W_e^{(0)} = W_e^{SR} + 2j^{GG}(\omega_0)B_0^2 + X \qquad (10)$$

with X ascribed to intramolecular rotationally independent processes, and contributions from dipolar terms with solvent nuclei are estimated to be small.[2a] To that purpose the Zeeman (G) contribution, which can be accurately estimated from available $j^{DD}(\omega_0)$ and $j^{DG}(\omega_0)B_0$ terms, is subtracted from $W_e^{(0)}$. Next, the residual is plotted vs. T/η as shown in Figure 6 for TO, SBB, and MCH. This is suggested by the theory for W_e^{SR} in the strong interaction limit[17]

$$W_e^{SR} = (1/3) \sum_{i=x,y,z} (g_{ii} - 2.00231)^2 R_i \qquad (11)$$

TABLE VII: Spectral Densities $j(\omega)$ and Transition Probabilities W for PDT in TO, SBB, MCH, and 8CB[a]

solvent	T, K	$10^5 W_e^{(0)}$, s^{-1}	$10^5 j_{(0)}^{DD}$, s^{-1}	$10^5 j_{(\omega_n)}^{DD}$, s^{-1}	$10^5 j_{(0)}^{DG} \cdot B_0$, s^{-1}
TO	233	3.03	1.19	1.18	0.34
	223	2.83	1.79	1.87	0.56
	216	2.30	2.45	2.30	0.77
	211	2.00	2.84	2.65	0.94
	204	1.55	3.94	3.72	1.28
	198	1.29	5.26	5.00	1.74
	193	1.13	6.94	6.58	2.33
	188	0.94	9.72	9.78	3.19
SBB	238	3.50	2.27	2.14	0.78
	235	3.17	2.52	2.46	0.87
	230	2.77	3.13	3.26	1.03
	225	2.05	3.87	3.64	1.38
	223	2.19	4.33	4.29	1.49
	220	1.70	5.08	4.86	1.78
	215	1.42	6.69	6.67	2.35
	210	1.26	9.66	10.28	3.25
MCH	206	3.28	2.01	1.67	0.65
	199	2.64	2.46	2.16	0.73
	193	2.25	3.11	2.54	0.98
	186.5	1.77	4.29	3.72	1.33
	179.5	1.25	5.20	4.09	1.57
	173	1.07	7.41	6.32	2.16
8CB	324	4.93	5.30	4.43	1.73
	320	4.23	6.75	5.18	2.23
	317	4.18	8.44	5.32	2.81

[a] Estimated accuracies: $W_e^{(0)}$ (8%), $j^{DD}(0)$ (5%), $j^{DD}(\omega_n)$ (10%), $j^{DG}(0)B_0$ (5%). [b] The uncertainties in the $j(\omega)$ and $W_e^{(0)}$ are partly correlated. Estimated accuracy in $j^{DD}(0)/j^{DD}(\omega_n)$ is ±7%.

with R_i proportional to the temperature (T)/viscosity (η) ratio.

For the limited data in 8CB the W_e^{SR} results (4.29×10^5, 3.61×10^5, and 3.56×10^5 s^{-1} at 324, 320, and 317 K) were obtained by taking $X = 5 \times 10^4$ s^{-1} which was based upon the fairly constant X value found in TO, SBB, and MCH (see caption to Figure 6) and observed elsewhere[6] for PDT at the very low $T/\eta = 50$ K/P.

RD vs. SRLS. For TO and SBB the results in Table VII point to $j^{DD}(0) = j^{DD}(\omega_n)$, in contrast to MCH and 8CB where always $j^{DD}(0) > j^{DD}(\omega_n)$ was observed. In plots of $j^{DD}(0)$ vs. η/T (Figure 7, solid lines) TO and SBB show the well-known linear relationship with an approximately zero intercept. For MCH and 8CB large deviations from this behavior are found. In the plot for 8CB the viscosity data[19] for the closely related 7CB compound were used. The dashed lines represent analysis of results to be explained later.

These facts do suggest that for MCH and 8CB the relaxation mechanism is more complicated than simply RD. The inequality of j^{DD} terms, while being far in the motional narrowing region, can be understood by SRLS-type contributions with $\tau_X \approx \omega_n^{-1}$. In TO and SBB RD is sufficient to explain the results although SRLS with $\tau_X \ll \omega_n^{-1}$ cannot be excluded. The above considerations indicate that an unambiguous separation of RD- and SRLS-type contributions is essential for further analysis. In that context the relaxation data for TO, SBB, and MCH in Table VII are considered in a preliminary approach. Some results related to the extreme and a few intermediate temperatures are summarized in Table VIII and are explained hereafter.

In TO and SBB standard analysis[1] of the various $j(\omega)$ in terms of RD yields data for $\bar{\tau}$ and N_α at each temperature, and then

(17) (a) R. E. D. McClung, *J. Chem. Phys.*, **75**, 5503 (1981); (b) P. Atkins, "Electron Spin Relaxation in Liquids", L. T. Muus and P. W. Atkins, Eds., Plenum Press, New York, 1972 Chapter XI.

(18) Viscosity results for TO and SBB from A. J. Barlow, J. Lamb, and A. J. Matheson, *Proc. R. Soc. London, Ser. A*, **292**, 322 (1966), and for MCH from G. A. von Salis and H. Labhart, *J. Phys. Chem.*, **72**, 752 (1968).

(19) S. D. Hunisitt and J. C. A. van der Sluis, *J. Phys. Lett.*, **44**, L59 (1983).

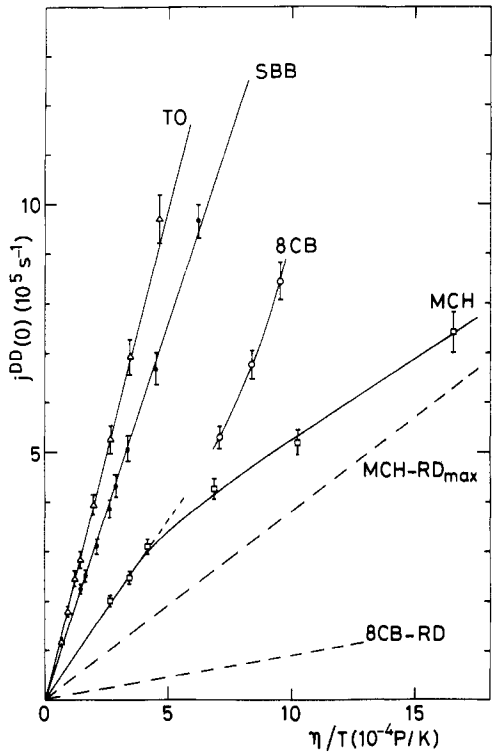

Figure 7. Experimental (—) plots of $j^{DD}(0)$ vs. η/T for PDT in TO, SBB, MCH, and 8CB. The dashed curves refer to evaluated $j_{RD}{}^{DD}(0)$ vs. η/T in MCH and 8CB. See text.

TABLE VIII: RD Analysis Results for PDT in TO, SBB, and MCH

solvent	T, K	$N_\alpha{}^a$	$10^{-11}\bar{\tau}$,[b] s	ϵ^c	ΔW_e^{SR},[d] %
TO	233	2.6	1.52	1.9	13
	216	1.6	3.03	1.7	36
	204	1.3	4.81	1.4	28
	188	1.2	11.81	0.8	35
SBB	238	1.4	2.74	2.2	50
	225	1.4	4.66	1.7	38
	220	1.6	6.12	1.3	41
	210	1.3	11.65	1.0	56
MCH	206	1.35	1.26	2.7	8
	193	1.35	2.31	2.5	3
	173	1.35	7.89	1.0	7

[a] TO ($\alpha = y$); SBB ($\alpha = x$); MCH ($\alpha = y$). Accuracy ±20%. [b] Accuracy ±7%. [c] Accuracy ±0.5. [d] $\Delta W_e^{SR} = [W_e^{SR}(\text{expt}) - W_e^{SR}(\text{calcd})]/W_e^{SR}(\text{expt})$.

one can compared calculated (cf. eq 10) with experimental W_e^{SR} values. The results given for MCH require somewhat more explanation. The nonlinearity in Figure 7 together with the inequality $j^{DD}(0) > j^{DD}(\omega_n)$, while the normal T/η dependence (Figure 6) is still noticed, do suggest that the spectral densities of PDT in MCH consist of an RD portion which is linear in η/T and an SRLS portion with different behavior. The upper limit of the RD part is estimated by ascribing $j^{DD}(\omega_n) = 6.32 \times 10^5$ s^{-1} at 173 K (Table VII) fully to RD and by extrapolating then via linear η/T behavior to the other temperatures. This result is represented by the dashed line (MCH RD_{max}) in Figure 7. It shows that the lower limit of SRLS-type contributions in $j^{DD}(0)$ varies from 50% at 206 K to about 15% at 173 K. For a given assumption of N_α the upper limit of $j_{RD}^{DD}(0)$ can be analyzed in the standard manner[1] to yield values for $R_\parallel$ and $R_\perp$, and afterward a comparison between calculated (eq 10) and experimental W_e^{SR} data can be made. N_α is varied until optimum agreement in W_e^{SR} is obtained. The final outcome of $N_y \approx 1.35$ is very reasonable in view of the almost spherical PDT molecule. The ϵ values are obtained from standard analysis[1a] of $j^{DD}(\omega_0)$ in terms of 100% RD which is justified by $\tau_X \gg \tau_i > \omega_0^{-1}$. It is pointed out that for lower estimates of $j_{RD}{}^{DD}(0)$ the optimum fit shifts to larger N_y values which seems somewhat less probable.

The rather unambiguous separation of SRLS and RD contributions in MCH leads to a strikingly better fit in W_e^{SR} than obtained in TO and SBB with 100% RD. More generally, it suggests W_e^{SR} (cf. eq 10) to be a valuable probe for RD contributions. It might be helpful to solve the ambiguity noticed in the literature on W_e^{SR} analysis[1b,2a,20] in the motional region 10^{-11} s < $\bar{\tau}$ < 10^{-9} s: On one hand, the always large discrepancy in W_e^{SR} is ascribed to a breakdown of the Hubbard–Einstein relation

$$\tau_J \tau = I/6kT \tag{11}$$

as a theoretical basis for W_e^{SR} (cf. 10). I is the moment of inertia, τ_J the correlation time of angular momentum, and k the Boltzmann constant. On the other hand, theoretical formulations,[17] also the most recent one in terms of the fluctuating torque model,[2a,3] show (11) to be essentially correct. Stillman et al.[21] suggest that SRLS may be an alternative explanation in this matter. In that context the MCH result seems to be the first experimental support to their statement. The results in MCH show moreover that a virtually normal η/T behavior of $j^{DD}(0)$ (cf. Figure 7, above 190 K) can be indeed the resultant of two viscosity controlled dynamical processes. It emphasizes the option for SRLS-type contributions in solvents like TO and SBB in order to explain the otherwise large misfit in W_e^{SR} analysis.

From the above point of view the question of RD vs. SRLS contributions in TO and SBB can be considered somewhat more quantitatively via the role of the diffusion constants[2a]

$$R_i = \frac{k}{8\pi a^3 \sigma_i \kappa_i} \frac{T}{\eta} \quad (i = \parallel, \perp) \tag{12}$$

in the linear plots of Figures 6 and 7. The σ_i and a are structural constants for the PDT molecule. The κ_i are empirical parameters[22] with

$$0 < \kappa_i \leq 1 \tag{13}$$

which account for deviations from the ideal Stokes–Einstein model ($\kappa_i = 1$) due to hydrodynamic slip. In view of the almost spherical PDT the variation in the slopes in Figures 6 and 7 can be shown to arise mainly from differences in $\bar{\kappa} = (\kappa_\parallel \kappa_\perp)^{1/2}$. From Figure 6 the $\bar{\kappa}$ ratio is found to be TO:SBB:MCH = 3:2:1 whereas from the $j^{DD}(0)$ plots 5:4:1 is obtained. Consistency is restored if about 30% (TO) and 50% (SBB) of $j^{DD}(0)$ is ascribed to SRLS. These portions can be modified somewhat by small differences in N_α. A more detailed analysis is not feasible because it would require further specification of the SRLS mechanism which is rather speculative in view of the unknown solvent structure around the spin probe. It is pointed out that consequently the actual characterization of RD has become somewhat uncertain. The N_α in Table VIII may be considered only as a rough indication while the actual ϵ values will be somewhat larger than given there.

The relaxation results in 8CB can be considered in more detail. With $g_{zz} = 2.0022$, W_e^{SR} is practically (cf. eq 10) a two-parameter function $f(R_x,R_y)$. A particular choice for R_y fixes the R_x values and on the assumption of axially symmetric RD one can calculate $j_{RD}{}^{DD}(0) = j_{RD}{}^{DD}(\omega_n)$ and $j_{RD}{}^{DG}(0)B_0$. After subtraction from the corresponding overall $j^{XY}(\omega)$ in Table VII the respective $j_{SRLS}{}^{XY}(\omega)$'s remain. One finds throughout large dominating (80–90%e SRLS portions which are almost invariant over a large range of R_y values and can be described by[2c,23]

$$j_{SRLS}^{XY}(\omega) = (1/5) \sum_{K=-2}^{2} \sum_{K'=-2}^{2} X_K Y_{K'} \langle S_{l_K} S_{l_{K'}} \rangle \frac{\tau_X}{1 + \omega^2 \tau_X{}^2} \tag{14}$$

(20) D. S. Leniart, H. D. Connor, and J. H. Freed, *J. Chem. Phys.*, **63**, 165 (1975).
(21) A. E. Stillman and R. N. Schwartz, *J. Phys. Chem.*, **85**, 3031 (1981).
(22) R. E. D. McClung and D. Kivelson, *J. Chem. Phys.*, **49**, 3380 (1968).

TABLE IX: RD and SRLS Analysis Results for PDT in 8CB

T, K	N_α[a]	$10^{-12}\bar{\tau}$,[b] s	ϵ[c]	$\langle S_{l_0}^2\rangle^{1/2}$[d]	$10^{-9}\tau_X$,[e] s
324	2.3	8	1.2	0.12	3.8
320	1.5	10	2.8	0.12	4.8
317	1.1	11	2.9	0.12	6.7

[a] $\alpha = y$; accuracy ±40%. [b] Accuracy ±10%. [c] Accuracy ± 0.5%. [d] Accuracy ±7% (for $X = 5 \times 10^4$ s^{-1}). [e] Accuracy ±5% (for $X = 5 \times 10^4$ s^{-1}).

TABLE X: Thermodynamic Parameters for PDT in TO, SBB, MCH, and 8CB

solvent	process	E_a, kcal/mol	ln $\bar{\tau}_0$
TO[a]	RD	3.6 ± 0.2	−33.1 ± 0.4
SBB[a]	RD	5.0 ± 0.7	−36 ± 2
MCH[a]	RD	4.0 ± 0.3	−35.1 ± 0.8
8CB[b]	RD	9.3 ± 0.9	−40 ± 1
8CB[b]	SRLS	16.3 ± 1.6	−45 ± 3

[a] The errors are from least-squares analyses. [b] The errors are estimated, since only three temperatures are available.

with X_K, $Y_{K'}$ the Kth and K'th spherical tensor components of the interactions X and Y in the SRLS principal axis system. The quantities $\langle S_{l_K} S_{l_{K'}}\rangle$ are an average over fluctuations in S_{l_K} and $S_{l_{K'}}$, the irreducible tensor components of the local ordering. The experimental result $j_{SRLS}^{DD}(0)/(j_{SRLS}^{DG}(0)B_0) = 3.00 \pm 0.05$ over a large range of R_y values allows one to reduce eq 14 considerably[24] and only the $K = 0$ term remains with the molecular z axis as principal z axis in the SRLS reference frame. Straightforward analysis of all $j(\omega)$ terms yields τ_X, $\langle S_{l_0}^2\rangle$, $\bar{\tau}$, and ϵ for each initial choice of R_y. In Table IX the numerical outcome is summarized for $j_{SRLS}^{DD}(0)/(j_{SRLS}^{DG}(0)B_0)$ being exactly 3.00. The $j_{RD}^{DD}(0)$ data are included in Figure 7 (dashed curve, 8CB RD).

Activation Energies. On the assumption of a temperature dependence of $\bar{\tau}$ according to

$$\bar{\tau} = \tau_0 e^{-E_a/kT} \tag{15}$$

with E_a the activation energy, one finds the results collected in Table X after separation of the RD and SRLS portions (N_α, cf. Table VIII, see previous section). The E_a values for TO, SBB, and MCH are usual for hydrocarbon solvents. The TO result is similar to the value 3.9 kcal/mol found elsewhere.[2a] The E_a in 8CB is largely different from the result of Lin et al.[2c] (14.1 kcal/mol) which was based upon a 100% RD approach. The τ_X values in 8CB were analyzed similarly. The E_a value for SRLS is significantly larger but not unreasonable in view of the larger molecular scale. The ln τ_0 values are in the usual range as found elsewhere.[2c]

Further Discussion

The general result of our approach is that the rotational relaxation arises from RD and SRLS type contributions. This raises the question of physical significance, particularly in the ordinary liquids TO, SBB, and MCH. The sequence of $\bar{\kappa}$ values in these solvents points to a hydrodynamic slip in the order MCH > SBB > TO. It suggests that the PDT probe reorients in a solvent structure which is correspondingly more quasistatic on the rotational time scale. From the SRLS point of view a similar conclusion can be drawn: the solvent structure in MCH is most rigid ($\tau_X \approx \omega_n^{-1}$) and apparently more flexible in the other solvents ($\tau_X \ll \omega_n^{-1}$) but with a significantly larger contribution in SBB than in TO. It was pointed out by Zager et al.[2d] that any relaxation process whose correlation function is expressed as the sum of two exponentials (τ_i and τ_X) may be written quite generally in the form of eq 1, 2, and 14. Then, from a physical point of view one might suppose that in the solvents TO, SBB, and MCH the SRLS mechanism represents a rather slow modulation of the hydrodynamic slip determining properties of the solvent. Certain results on MCH (see Figure 7, Table XI) may further indicate that the solvent matrix becomes increasingly rigid toward lower temperatures and induces ultimately the conformational effects noted in the rigid limit spectra (Figure 2, a and b): Firstly the SRLS portion in $j^{DD}(0)$ goes through a maximum (cf. Figure 7) and at the lowest temperatures merely secular contributions are left, indicating $\tau_X \gg \omega_n^{-1}$. Secondly, the electron spin exchange rate W_{ex} increases toward lower temperatures (see Table XI) whereas normally (as observed in TO and SBB) a decrease is expected. It points to increased translational diffusion or clustering of radicals. In that respect it resembles EPR results on glass formation[14] and freezing.[1a] With increasing W_{ex} one should be aware of contributions from an intermolecular electron spin dipolar origin,[24] which in this study is most relevant to $W_e^{(0)}$. In Figure 6 no anomalous increase of the electron spin relaxation rate toward lower temperatures can be discerned and therefore this mechanism is thought to be of minor importance.

TABLE XI: Electron Spin Exchange Rate W_{ex} for PDT in MCH

T, K	$10^4 W_{ex}$,[a] s^{-1}	T, K	$10^4 W_{ex}$,[a] s^{-1}
206	1.64	186.5	3.18
199	1.85	179.5	4.51
193	2.48	173	7.09

[a] Accuracy ±20%.

In 8CB the physical background of the SRLS mechanism can be related somewhat more directly to local ordering properties. The quantity $\langle S_{l_0}^2\rangle^{1/2}$ is found to be fairly constant, is on the order of the static value in the S_A phase at 303 K, and does suggest that the ordering property of 8CB might already be present in the isotropic phase but then on a microscopic scale. The τ_X values for PDT in 8CB correspond within a factor of 2 to the $R_\perp$ values of long rodlike spin probes[13] inferred from relaxation measurements in the isotropic phase of the closely related solvent 5CB. This supports the concept of an SRLS process in 8CB as due to the perpendicular modes[5] in the solvent molecules.

Conclusions

The saturation and ELDOR results are incompatible with line-width results when the latter are interpreted in the standard manner[2] by axially symmetric rotational diffusion with a temperature invariant N_α and ϵ.

In a more general approach it is shown that all spectral densities $j(\omega)$ and the rates $W_e^{(0)}$ and W_{ex} can be obtained independently from the combined line-width, T_1, and ELDOR results.

A comparative analysis of the relaxation terms $j(\omega)$ and $W_e^{(0)}$ in TO, SBB, and MCH strongly suggests that, in general, the reorientation of PDT can be ascribed to RD and SRLS contributions. In that view the spin–rotational interaction term W_e^{SR} seems to be a valuable probe for RD contributions. Referring to discussions elsewhere[2] it is pointed out that, beside the SRLS contribution, the general approach still requires $N_\alpha > 1$ and $\epsilon > 1$ for the more or less spherical PDT molecule.

The RD–SRLS approach to 8CB does suggest that the ordering observed at lower temperatures in the smectic S_A phase is already present in the isotropic phase but then on microscopic scale. The observed τ_X values support the SRLS mechanism as due to perpendicular modes in the rodlike solvent molecules. In view

(23) As pointed out by Hwang et al.[5] the frequency dependence for secular and pseudosecular SRLS terms in the motional region $\tau_X \approx \omega_n^{-1}$ is in fact a little more subtle than suggested in eq 16. The basic theory for this is given by Hwang et al.[2a] and extended to SRLS by Polnaszek et al.[2b] In this work, however, the simplified formula (eq 16) is sufficient since S_l turns out to be small (≈0.1).

(24) In analogy to results[2c] in the smectic and nematic phases of 8CB it is reasonable to assume that the molecular z axis orients perpendicular to the local director, and given that the fundamentally slow ($\tau_X \gg \tau_i$) relaxation of the local structure is governed by the most improbable reorientation of the long rodlike solvent molecules about axes perpendicular to the long axis or local director,[5] this z axis forms then a natural choice for the princpal z axis in the SRLS reference frame. In view of a nearly axially symmetric A only $K = 0$ terms are then important. Cross terms are not considered. Straightforward substitution in (15) yields $(j_{SRLS}^{DD}(0)/j_{SRLS}^{DG}(0))B_0 = 2.99$, which is close to the experimental value.

of the 8CB results the combined T_2-T_1-ELDOR method seems promising in research on ordering media by its option to yield directly the ordering dynamics of the nearby environment.

Acknowledgment. The authors thank Dr. Rassat (Grenoble) for his generous gift of PDT when this project started.

Appendix

In the parameter set

$$\overline{j^{DD}}(\omega_n), \qquad \overline{j^{DD}}(\omega_0), \qquad \overline{j^{DG}}(\omega_0)B_0, \qquad \overline{W_{ex}} \qquad \text{(A.1)}$$

one has in the standard formulation,[1a] over a large range of N_α and $\bar{\tau}$

$$2.6 < \overline{j^{DD}}(\omega_0)/(\overline{j^{DG}}(\omega_0)B_0) < 3.4 \qquad \text{(A.2)}$$

for $1 < N_\alpha < 3$ and $\bar{\tau} < 10^{-9}$ s. So it is most useful to start the ELDOR analysis with a fixed value of this ratio and to refine it afterward if the final outcome would make this necessary. Similarly $\bar{W}_{ex}$ can be added afterward in view of the small experimental deviations from eq 5. Finally, two independent parameters are left: $\overline{j^{DD}}(\omega_n)$ and $\overline{j^{DD}}(\omega_0)$. By variation one finds an unambiguous optimum ELDOR fit which can be refined somewhat by adding $\bar{W}_{ex}$. As a second step in the approach $W_e^{(0)}$ is determined from the experimental $T_1^{(m)}$ and the dimensionless products $T_1^{(m)}W_e^{(0)}$ which are calculated simultaneously with the ELDOR reduction factors. Finally, if further analysis of $j(\omega)$ and $W_e^{(0)}$ together would yield rotational diffusion results which are incompatible with the initial selection of the ratio (A.2), the solution can be refined by iteration. Since the more or less spherical PDT reorients nearly isotropically, a convenient starting value is 3.0. Considering the experimental accuracies further iteration is not needed.

Registry No. PDT, 36763-53-8.

Ligand (Adsorbate) Substitutions at Metal Surfaces: Aromatic Compounds and Halides at Smooth Polycrystalline Platinum Electrodes

Manuel P. Soriaga,* James H. White, Dian Song, and Arthur T. Hubbard*

Department of Chemistry, University of California, Santa Barbara, California 93106
(Received: December 27, 1983)

Ligand (adsorbate) substitution reactions between aromatic compounds and halides at smooth polycrystalline Pt surface in solution have been studied. Adsorption and desorption measurements were based on thin-layer electrochemical techniques. Hydroquinone (HQ) was studied with F^-, Cl^-, and Br^-; 1,4-naphthohydroquinone (NHQ) with Br^- and I^-. The ease of displacement of preadsorbed halide by HQ decreased in the order $F^- >> Cl^- > Br^-$; adsorbed I was completely inert. The ease of desorption of preadsorbed HQ by halide decreased in the order $\eta^2 > \eta^6$, and $Br^- > Cl^-$; F^- was unable to displace adsorbed HQ. Displacement of η^{10} and η^2 NHQ by 10 mM I^- at −0.100 V (vs. AgCl in 1 M H^+) was virtually quantitative. Halide-induced aromatic desorption increased when the potential was decreased, although at −0.200 V hydrogenation processes accompanied the displacement reactions. Species not desorbed retained their initial orientations. Competitive adsorption between HQ and the halides yielded results similar to HQ adsorption on halide pretreated surfaces; the adsorption profiles suggested flat orientations at HQ concentrations < 0.5 mM and edge orientations at > 1.0 mM. Results on competitive adsorption between NHQ and I^- indicated that, in contrast to the other halides, I^- is sufficiently surface active to enforce molecular reorientations even at comparatively low aromatic concentrations.

Introduction

Aromatic molecules are spontaneously and irreversibly adsorbed on smooth polycrystalline Pt electrodes.[1] The organometallic chemisorptive interactions are unimpeded by the presence of weakly coordinating solvents (water) or anions (ClO_4^-, PF_6^- HSO_4^-, SO_4^{2-}, $H_2PO_4^-$, HPO_4^{2-}, PO_4^{3-}).[1m] The inability of these aqueous electrolyte solutions to interfere with irreversible adsorption has also been demonstrated on structurally and chemically well-defined Pt single-crystal surfaces.[2-4] When an organic monolayer was allowed to interact with iodide/iodine[5-7] solutions, displacement and/or reorientation of the initially adsorbed organic along with halogen coadsorption were observed.[1b,3]

Displacement reactions between halides and aromatic compounds at smooth polycrystalline Pt in aqueous solutions, analogous to ligand substitution reactions in molecular coordination compounds, are described in the present paper: (1) adsorption of aromatics on halide-pretreated surfaces in relation to the ease of displacement of preadsorbed halide; (2) displacement of preadsorbed aromatic by halides including the influence of adsorbed aromatic orientation, halide concentration, and electrode potential; (3) competitive adsorption from solutions containing various proportions of aromatic and halides. Hydroquinone (HQ) and 1,4-naphthohydroquinone (NHQ) were employed as model aromatic compounds since the adsorptive properties of these substances on Pt have been studied extensively.[1]

Experimental Section

The measurement of absolute surface coverages based on thin-layer coulometry[8] has been described.[1c,e,n] The amount ad-

(1) (a) Soriaga, M. P.; Hubbard, A. T. *J. Am. Chem. Soc.* **1982**, *104*, 2735. (b) *Ibid.* **1982**, *104*, 2742. (c) *Ibid.* **1982**, *104*, 3937. (d) Soriaga, M. P.; Wilson, P. H.; Hubbard, A. T.; Benton, C. S. *J. Electroanal Chem.* **1982**, *142*, 317. (e) Chia, V. K. F.; Soriaga, M. P.; Hubbard, A. T.; Anderson, S. E. *J. Phys. Chem.* **1983**, *87*, 232. (f) Soriaga, M. P.; White, J. H.; Hubbard, A. T. *Ibid.* **1983**, *87*, 3048. (g) Stickney, J. L.; Soriaga, M. P.; Hubbard, A. T.; Anderson, S. E. *J. Electroanal. Chem.* **1981**, *125*, 73. (h) Soriaga, M. P.; Stickney, J. L.; Hubbard, A. T. *Ibid.* **1983**, *144*, 207. (i) *J. Mol. Catal.* **1983**, *21*, 211. (j) Soriaga, M. P.; Hubbard, A. T. *J. Electroanal. Chem.* **1983**, *159*, 101. (k) *J. Phys. Chem.*, in press. (l) *Ibid.*, **1984**, *88*, 1089. (m) Soriaga, M. P.; Chia, V. K. F.; White, J. H.; Song, D.; Hubbard, A. T. *J. Electroanal. Chem.*, in press. (n) Soriaga, M. P.; Hubbard, A. T. *Ibid.* in press. (o) Chia, V. K. F.; Soriaga, M. P.; Hubbard, A. T. *Ibid.*, in press.

(2) (a) Hubbard, A. T.; Stickney, J. L.; Rosasco, S. D.; Soriaga, M. P., Song, D. *J. Electroanal Chem.* **1983**, *150*, 165. (b) Stickney, J. L.; Rosasco, S. D.; Song, D.; Soriaga, M. P., Hubbard, A. T. *Surf. Sci.* **1983**, *130*, 326.

(3) Katekaru, J. Y.; Garwood, G. A.; Hershberger, J. F.; Hubbard, A. T. *Surf. Sci.* **1982**, *121*, 396.

(4) (a) Hubbard, A. T. *Acc. Chem. Res.* **1980**, *13*, 177. (b) *J. Vac. Sci. Technol.* **1980**, *17*, 49.

(5) Felter, T. E.; Hubbard, A. T. *J. Electroanal. Chem.* **1979**, *100*, 473.

(6) Garwood, G. A.; Hubbard, A. T. *Surf. Sci.* **1980**, *92*, 617.

(7) Lane, R. F.; Hubbard, A. T. *J. Phys. Chem.* **1975**, *79*, 808.

0022-3654/84/2088-2284$01.50/0